Topological Boundary Modes from Translational Deformations

Yosuke Nakata, Yoshitaka Ito, Yasunobu Nakamura, and Ryuichi Shindou

Phys. Rev. Lett. **124**, 073901 — Published 21 February 2020

DOI: 10.1103/PhysRevLett.124.073901

Topological boundary modes from translational deformations

Yosuke Nakata,[1,2,*] Yoshitaka Ito,[1] Yasunobu Nakamura,[1,3] and Ryuichi Shindou[4,5]

[1] *Research Center for Advanced Science and Technology (RCAST), The University of Tokyo, Meguro-ku, Tokyo 153-8904, Japan*
[2] *Graduate School of Engineering Science, Osaka University, Toyonaka, Osaka 560-8531, Japan*
[3] *Center for Emergent Matter Science (CEMS), RIKEN, Wako-shi, Saitama 351-0198, Japan*
[4] *International Center for Quantum Materials, Peking University, Beijing 100871, China*
[5] *Collaborative Innovation Center of Quantum Matter, Beijing 100871, China*

(Dated: January 27, 2020)

Localized states universally appear when a periodic potential is perturbed by defects or terminated at its surface. In this paper, we theoretically and experimentally demonstrate a mechanism that generates localized states through continuous translational deformations of periodic potentials. We provide a rigorous proof of the emergence of the localized states under the deformations. The mechanism is experimentally verified in microwave photonic crystals. We also demonstrate topological phase windings of reflected waves for translated photonic crystals.

In the 1930s, Tamm predicted the localized state of an electron near the surface of a solid [1]. Years later, Shockley proposed another mechanism that produces surface states, based on a band inversion of atomic orbitals [2]. Impurities and lattice defects inside a crystal also produce localized states [3, 4], which play important roles in doped semiconductors. While such localized states were first investigated for electrons, they universally appear in various wave systems. Zero-dimensional localized states have been observed in electronic superlattices [5], photonic and magnetophotonic crystals [6–8], plasmonic crystals [9–13], and phononic crystals [14].

The recent discovery of topological insulators has shed fresh light on the understanding of surface states in various wave systems from a topological perspective. Under time-reversal symmetry, bulk electronic states in band insulators are generally characterized by the Z_2 topological invariant [15, 16]. The bulk–edge correspondence relates the bulk Z_2 topological invariant to surface characteristics and ensures an existence of gapless boundary states with the Kramers degeneracy protected by time-reversal symmetry [17, 18]. Later, it was shown that other discrete symmetries and their combinations generate various topological numbers for bulk electronic states and associated in-gap gapless boundary states [19]. A pioneering example is the Z topological invariant with a sublattice symmetry in the Su–Schrieffer–Heeger (SSH) model [20, 21]. The non-zero topological integer in the SSH model ensures zero-energy end states with sublattice-symmetry protection. For continuous one-dimensional crystals with inversion symmetry, Xiao *et al.* established a relation between surface observables and bulk properties and rigorously determined the existence or nonexistence of localized states [22]. So far, research on one-dimensional systems has focused on unit cells with either sublattice or inversion symmetry to define the topological integers, but these discrete symmetries may not be essential, as suggested by Shockley [2]. In fact, the in-gap localized states as boundary states could survive under a gradual structural deformation that breaks the symmetries within the unit cell. This consideration indicates an alternative topological mechanism that generates localized states without using any symmetry protection.

In this letter, we devise a scheme that produces zero-dimensional localized states in a defect created by a translational deformation of a periodic potential. A rigorous proof of emergence of the localized states is provided without relying on any symmetry protection. The scheme is experimentally demonstrated in microwave photonic crystals.

Consider a one-particle eigenmode in one-dimensional continuous media with a periodic potential of the period a. From the Bloch theorem [23], the eigenmode $|\psi_n(k)\rangle = \exp(ik\hat{x})\,|u_n(k)\rangle$ is characterized by the crystal momentum k in the first Brillouin zone $[-\pi/a, \pi/a]$ and the energy band index n, where $\langle x|u_n(k)\rangle$ is periodic in x. For simplicity, we assume that the eigenenergy $E_n(k)$ of $|\psi_n(k)\rangle$ satisfies $E_1(k) < E_2(k) < \cdots$ in the entire Brillouin zone. From here, we focus on the n-th band. The first Brillouin zone is discretized as $k_i = i\pi/(Ma)$ with $i = -M+1, -M+2, \cdots, M$ ($2M$ points). In terms of $|u_i\rangle = |u_n(k_i)\rangle$, a Wilson loop is given by

$$W = \langle u_M|u_{M-1}\rangle\,\langle u_{M-1}|u_{M-2}\rangle \cdots \langle u_1|u_0\rangle \times \langle u_0|u_{-1}\rangle \cdots \langle u_{-M+2}|u_{-M+1}\rangle\,\langle u_{-M+1}|\mathrm{e}^{\mathrm{i}G\hat{x}}|u_M\rangle\,, \quad (1)$$

where $G = 2\pi/a$ and the inner product is defined in the unit cell [24]. It is normalized to be unity as $\lim_{M\to\infty} W = \exp(\mathrm{i}\theta_{\mathrm{Zak}})$, where θ_{Zak} is simply the Zak phase [25]. The Zak phase specifies a spatial displacement of the localized Wannier orbits that are composed only of the eigenmodes in the n-th energy band [24]. In electronic systems, the Zak phase corresponds to surface charge, which can take a fractional value [26–29].

Now, let us translate continuously the one-dimensional periodic potential by ξa ($0 \le \xi \le 1$) relative to a fixed frame of the unit cell. The spatial translation changes the potential configuration from U_0 to U_ξ inside the fixed

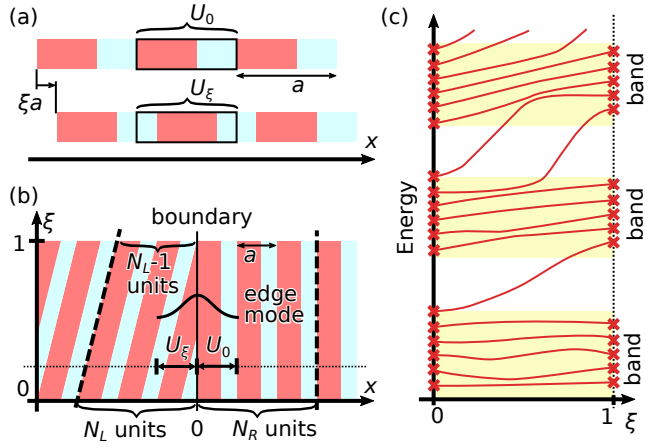

FIG. 1. (a) One-dimensional continuous medium with a periodic potential (upper) and the identical system with spatial translation by ξa (lower). (b) Spatial boundary between the two identical periodic systems with different translations. The Born–von–Karman (BvK) boundary condition is imposed, where the two dashed lines are identified with each other. (c) Eigenenergies of the entire system with the BvK boundary condition are schematically plotted as a function of the translational parameter ξ.

cell [see Fig. 1(a)]. When ξ changes from 0 to 1, the localized Wannier orbit is continuously translated by the periodic length a. Thus, it works like a classical screw pump [30]. Being identical to the displacement of the Wannier orbit with the unit-cell length (apart from a factor $2\pi/a$), the Zak phase also continuously increases by 2π under the translation: $\int_0^1 \mathrm{d}\xi\, \partial_\xi \theta_{\mathrm{Zak}} = 2\pi$. The phase winding counts the Chern integer, which represents the topological characteristics of a fiber bundle on the (k, ξ) plane [24, 31]. In this paper, ξ is regarded as a variable independent of other variables. Nonetheless, one could consider a continuous change of ξ as a function of time t. In particular, an adiabatic change of $\xi = \xi(t)$ from 0 to 1 in t suppresses interband transitions and is referred to as Thouless pumping [32].

The 2π phase winding in the Zak phase under the translation leads to a series of non-trivial localized states in a spatial boundary between two identical one-dimensional periodic systems with different translations ξ. To see this, let us consider a periodic arrangement of unit cells with U_ξ in a region of $x < 0$ and another periodic arrangement of unit cells with U_0 in the other region of $x \geq 0$. The translation parameter ξ and spatial coordinate x subtend an extended two-dimensional space, as shown in Fig. 1(b). When ξ changes from 0 to 1, the Zak phase in the former bulk region ($x < 0$) winds up the 2π phase. Meanwhile, the Zak phase in the latter bulk region ($x \geq 0$) remains unchanged. Accordingly, the bulk–edge correspondence [24, 31, 32] suggests the existence of zero-dimensional edge states at the boundary region ($x = 0$), whose eigenenergies have 'chiral' dispersions within a bulk band gap as a function of the translational parameter ξ [Fig. 1(c)]. Moreover, as the Zak phase for any bulk band in the region of $x < 0$ acquires the same 2π phase winding during the translation, the number of the 'chiral' dispersions between the n-th and $(n+1)$-th bulk bands are expected to be n [Fig. 1(c)].

To prove this bulk–edge correspondence in the translational deformation rigorously, let us impose the following Born–von–Karman (BvK) boundary condition on a finite system [Fig. 1(b)]. Suppose that at $\xi = 0$, the entire one-dimensional system is comprised of N_{L} unit cells in the region of $x < 0$ and N_{R} unit cells in the region of $x \geq 0$. For general ξ, we identify $x = -N_{\mathrm{L}}a + \xi a$ with $x = N_{\mathrm{R}}a$, such that the lattice periodicity is preserved at $x = N_{\mathrm{R}}a \equiv -N_{\mathrm{L}}a + \xi a$ and it is broken only at $x = 0$. For $\xi = 0$ and $\xi = 1$, the periodicity is completely preserved in the entire system, so that the eigenmodes at $\xi = 0$ and $\xi = 1$ are all spatially extended bulk band states. Under the BvK boundary condition, which discretizes the Brillouin zone, numbers of the bulk modes in each band at $\xi = 0$ and at $\xi = 1$ are given by $N_{\mathrm{L}} + N_{\mathrm{R}}$ and $N_{\mathrm{L}} + N_{\mathrm{R}} - 1$, respectively. Namely, the number of the extended bulk states decreases by one in each band when ξ continuously changes from 0 to 1. As the energy has a lower bound and there is no upper bound on the bulk band index n in continuous media, more than one eigenmode in each bulk band at $\xi = 0$ must move into bulk bands with a higher energy at $\xi = 1$ during the translation of ξ. For example, when one eigenmode in the lowest bulk band at $\xi = 0$ goes to the second lowest bulk band at $\xi = 1$, two eigenmodes in the second lowest band at $\xi = 0$ must go to the third lowest one at $\xi = 1$ [Fig. 1(c)]. This argument inductively dictates that during the translation of ξ, n modes always raise their energies out of the n-th bulk energy band and go across the band gap between the n-th and $(n+1)$-th bands. An in-gap mode generally has a complex-valued wavenumber [33]. Accordingly, the n in-gap modes must be spatially localized at $x = 0$, where the lattice periodicity is broken; therefore, they are simply defect modes localized at the boundary. Importantly, the argument so far does not require any symmetry protection for the presence of the in-gap localized states.

Now, we experimentally confirm the theoretical concept by using microstrip photonic crystals. A microstrip is a transmission line composed of a metallic strip separated from a conducting ground plane by a dielectric substrate. Microwaves propagate between the topside metallic strip and the backside ground plane, and the impedance and refractive index of a microstrip are determined by the geometrical parameters.

The first photonic system studied has a binary unit cell, in which the two strips with different widths behave as two different media. As shown schematically in Fig. 2(a), we continuously introduce a defect around the boundary by displacing the left half by ξa while leaving

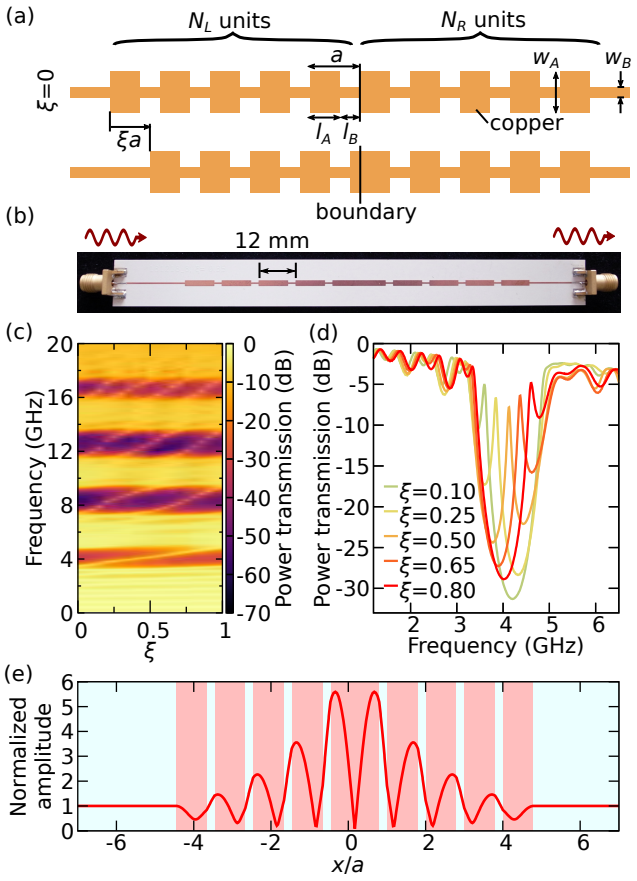

FIG. 2. (a) Schematic top view of binary microstrips at $\xi = 0$ (upper) and at $\xi \neq 0$ (lower). (b) Photograph of a sample with $\xi = 0.35$. The structural parameters are $a = 12\,\mathrm{mm}$, $l_\mathrm{A}/a = 0.8$, $l_\mathrm{B}/a = 0.2$, $w_\mathrm{A} = 1.8\,\mathrm{mm}$, $w_\mathrm{B} = 0.45\,\mathrm{mm}$, and $N_\mathrm{L} = N_\mathrm{R} = 5$. The microstrip is made of a $35\,\mu$m-thick copper film on a polyphenylene-ether substrate (Risho CS-3396; thickness 0.56 mm, $\epsilon = 11.3$, $\tan\delta = 0.003$ at 1 GHz), and SMA connectors (GigaLane PSF-S01-001) are attached to the substrate. The back of the substrate contains a ground plane made of a copper film with the same thickness as the microstrip. (c) Power transmission spectra through the 21 samples from $\xi = 0$ to $\xi = 1$ with the step size of $\Delta\xi = 0.05$. The input power is set to 0 dBm. (d) Power transmission spectra inside the first band gap for several values of ξ. (e) Calculated distribution of the absolute value of the complex electric-field amplitude at 4.22 GHz with $\xi = 0.538$ inside the first band gap. The amplitude is normalized to that of the incident field. Regions of different colors represent different width strips.

the right half unchanged. A photograph of one of the fabricated samples ($\xi = 0.35$) is provided in Fig. 2(b). Using a vector network analyzer (Keysight 5232A), we measured the power transmission through the samples with ξ from 0 to 1 with a step size of $\Delta\xi = 0.05$. The transmission spectra obtained for these different ξ are summarized in Fig. 2(c). Under 20 GHz, we clearly see five transmission bands, and four band gaps between them. The n-th band gap has n boundary modes running between the two neighboring transmission bands, as expected from

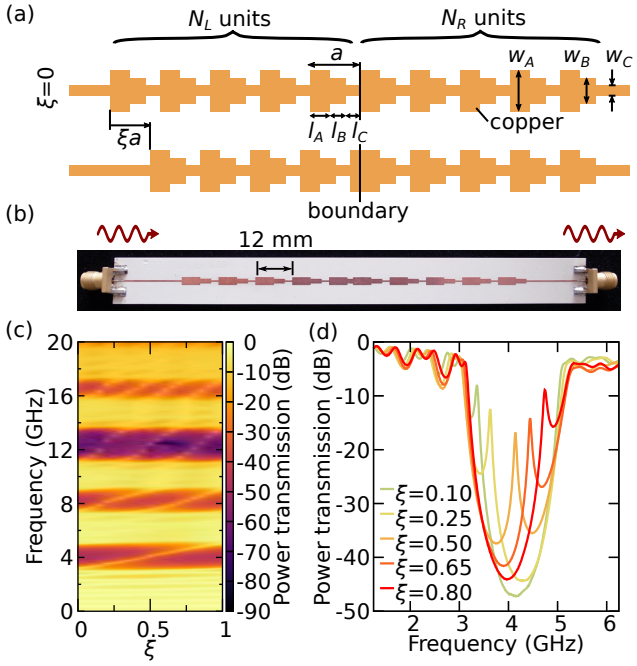

FIG. 3. (a) Schematic top view of ternary microstrips at $\xi = 0$ (upper) and at $\xi \neq 0$ (lower). (b) Photograph of a sample with $\xi = 0.35$. The structural parameters are $l_\mathrm{A}/a = 0.5$, $l_\mathrm{B}/a = 0.3$, $l_\mathrm{C}/a = 0.2$, $w_\mathrm{A} = 2.5\,\mathrm{mm}$, $w_\mathrm{B} = 1.5\,\mathrm{mm}$, and $w_\mathrm{C} = 0.45\,\mathrm{mm}$. The other parameters are the same as those in Fig. 2. (c) Power transmission spectra through the 21 samples from $\xi = 0$ to $\xi = 1$ with a step size of $\Delta\xi = 0.05$. (d) Power transmission spectra inside the first band gap for several values of ξ.

the theory. The qualitative behavior of the transmission spectra can be well captured by a transfer-matrix model calculation [34]. Figure 2(d) shows some of the experimentally obtained power transmission spectra inside the first band gap. The transmission peak decreases and the line width becomes narrower around $\xi = 0.50$. This is because coupling between the incident wave and the boundary mode is reduced at the center of the band gap. In fact, the transfer-matrix model calculation confirms that the localized mode becomes the narrowest at the center of the first band gap [34], as plotted in Fig. 2(e).

The second photonic system studied has three components in the unit cell. The design and photograph of the ternary microstrips are shown in Figs. 3(a) and (b), respectively. With three different material regions, the unit cell has no spatial inversion symmetry at any ξ. Figures 3(c) and (d) illustrate the experimental transmission spectra for 21 samples with different ξ [34]. These transmission spectra confirm that the n localized modes run across the n-th transmission gap during the translation of ξ from 0 to 1. The experimental results clearly demonstrate that inversion symmetry is not essential for the generation of the series of localized states through translational deformation.

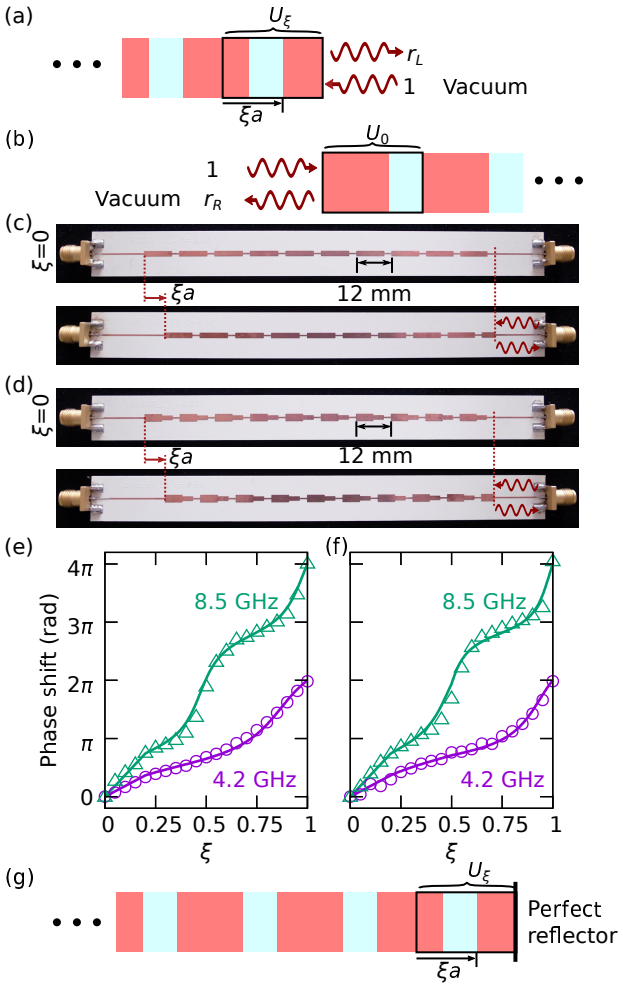

FIG. 4. Definitions of (a) left and (b) right complex reflection amplitudes $r^{(\mathrm{L})}(\xi,\omega)$ and $r^{(\mathrm{R})}(\omega)$, respectively. Photograph of (c) binary and (d) ternary samples ($\xi = 0$ and 0.60) to measure $r^{(\mathrm{L})}(\xi,\omega)$. The parameters are the same as those in Figs. 2 and 3. Topological winding of $\arg[r^{(\mathrm{L})}(\xi,\omega_0)] - \arg[r^{(\mathrm{L})}(0,\omega_0)]$ as a function of ξ for (e) binary and (f) ternary samples. Here, ω_0 is set to $2\pi \times 4.20$ GHz and $2\pi \times 8.50$ GHz inside the first band gap (circles) and second band gap (triangles), respectively. A microwave is injected from the right connector; meanwhile, the left connector is connected to another port of the network analyzer through a cable. The theoretical curves for the semi-infinite systems are plotted with the experimentally obtained points. (g) One-dimensional photonic crystal terminated by a perfect reflector.

Next, we establish the physical origin of the localized states in terms of phase winding of the complex reflection amplitude. To this end, we divide the deformed crystal into two halves. Namely, the left region with U_ξ is now terminated at its right end by a vacuum region, while the right region with U_0 is terminated by the same vacuum region at its left end [Figs. 4(a) and (b)]. Photonic properties of each semi-infinite region are characterized by the complex reflection amplitude r or a relative surface impedance $Z_\mathrm{s} \equiv (1+r)/(1-r)$ at the respective termination. The topological characteristics of localized states are encoded between the complex reflection amplitudes at both terminations $r^{(\mathrm{L})}(\xi,\omega)$ and $r^{(\mathrm{R})}(\omega)$ with an angular frequency ω. Specifically, a condition for eigenmodes localized at the original defect is nothing but the resonance condition across the two terminations: $Z_\mathrm{s}^{(\mathrm{L})}(\xi,\omega) + Z_\mathrm{s}^{(\mathrm{R})}(\omega) = 0$. The resonance condition can also be written as $r^{(\mathrm{L})}(\xi,\omega) \cdot r^{(\mathrm{R})}(\omega) = 1$. When ω remains inside the band gap between the n-th and $(n+1)$-th bulk bands, both the semi-infinite regions behave as perfect reflectors: $|r^{(\mathrm{R})}(\omega)| = |r^{(\mathrm{L})}(\xi,\omega)| = 1$. Thus, the condition shows that the phase of $r^{(\mathrm{L})}(\xi,\omega)$ must wind up by $2\pi n$ during the translation from $\xi = 0$ to $\xi = 1$, because the n boundary modes move across the angular frequency ω in the gap. The direction of the winding is determined by Foster's theorem [34, 35].

The $2\pi n$ phase winding of the reflection is considered as the physical origin of the localized states. To confirm this phase winding experimentally, we fabricated samples composed only of the left-half parts with different ξ, as in Figs. 4(c) and (d). Figures 4(e) and (f) show measured phases of the reflected waves of samples with different ξ (relative to the measured phase at $\xi = 0$). The experimental data points agree well with the theoretical curves obtained from the transfer-matrix model calculations for the semi-infinite systems [34]. The results clearly demonstrate the presence of phase winding of the reflection amplitude, regardless of the unit-cell symmetry.

The phase winding of the reflection provides a unified perspective on both Tamm and Shockley states, which are often separately attributed to a perturbed surface potential and band inversion, respectively [1, 2, 8]. To this end, we consider that the left region with U_ξ is terminated by a perfect reflector at the right end as shown in Fig. 4(g). Given $|r^{(\mathrm{R})}(\omega)| = 1$ for those ω in the n-th transmission gap of the left part, the $2\pi n$ phase winding of $r^{(\mathrm{L})}(\xi,\omega)$ during the translation of ξ from 0 to 1 always guarantees the emergence of n localized eigenmodes at the termination, irrespective of the details of the reflector on the right side. This holds true for any reflector with ξ-independent perturbations, provided the perturbations maintain the perfect-reflection condition. Such perturbations include a delta-function-like surface perturbation, the existence of which distinguishes Tamm states from Shockley states, as discussed in Ref. 2. In this sense, our proposed mechanism provides a comprehensive viewpoint for both Tamm and Shockley states.

In summary, we demonstrated a scenario that produces localized states through translational deformations analogous to classical screw pumping. The mechanism is not restricted to a specific physical system; rather, it is universal for any waves. Localized states in a system, even in the absence of sublattice or inversion symmetry, are now interpreted as topological boundary modes. The termination at the spatial boundary is understood as an engi-

neered degree of freedom and can be used for tuning the spatial localization of the boundary mode.

The authors thank K. Usami, A. Noguchi, and M. W. Takeda for their fruitful discussions, and J. Koenig for his careful reading of the manuscript. This work was supported by JSPS KAKENHI (Grant No. 17K17777) and by the JST ERATO project (Grant No. JPMJER1601). RS was supported by NBRP of China Grants No. 2014CB920901, No. 2015CB921104, and No. 2017A040215.

* nakata@ee.es.osaka-u.ac.jp

[1] I. Tamm, Phys. Z. Sowjetunion **1**, 733 (1932).
[2] W. Shockley, Phys. Rev. **56**, 317 (1939).
[3] H. M. James, Phys. Rev. **76**, 1611 (1949).
[4] D. S. Saxon and R. A. Hunter, Philips Res. Rep. **4**, 81 (1949).
[5] H. Ohno, E. E. Mendez, J. A. Brum, J. M. Hong, F. Agulló-Rueda, L. L. Chang, and L. Esaki, Phys. Rev. Lett. **64**, 2555 (1990).
[6] P. Yeh, A. Yariv, and A. Y. Cho, Appl. Phys. Lett. **32**, 104 (1978).
[7] T. Goto, A. V. Dorofeenko, A. M. Merzlikin, A. V. Baryshev, A. P. Vinogradov, M. Inoue, A. A. Lisyansky, and A. B. Granovsky, Phys. Rev. Lett. **101**, 113902 (2008).
[8] A. P. Vinogradov, A. V. Dorofeenko, A. M. Merzlikin, and A. A. Lisyansky, Phys.-Usp. **53**, 243 (2010).
[9] H. Kitahara, T. Kawaguchi, J. Miyashita, and M. Wada Takeda, J. Phys. Soc. Jpn. **72**, 951 (2003).
[10] H. Kitahara, T. Kawaguchi, J. Miyashita, R. Shimada, and M. Wada Takeda, J. Phys. Soc. Jpn. **73**, 296 (2004).
[11] J. Guo, Y. Sun, Y. Zhang, H. Li, H. Jiang, and H. Chen, Phys. Rev. E **78**, 026607 (2008).
[12] M. E. Sasin, R. P. Seisyan, M. A. Kalitteevski, S. Brand, R. A. Abram, J. M. Chamberlain, A. Y. Egorov, A. P. Vasil'ev, V. S. Mikhrin, and A. V. Kavokin, Appl. Phys. Lett. **92**, 251112 (2008).
[13] G. C. Dyer, G. R. Aizin, S. J. Allen, A. D. Grine, D. Bethke, J. L. Reno, and E. A. Shaner, Nat. Photonics **7**, 925 (2013).
[14] M. Xiao, G. Ma, Z. Yang, P. Sheng, Z. Q. Zhang, and C. T. Chan, Nat. Phys. **11**, 240 (2015).
[15] C. L. Kane and E. J. Mele, Phys. Rev. Lett. **95**, 146802 (2005).
[16] L. Fu, C. L. Kane, and E. J. Mele, Phys. Rev. Lett. **98**, 106803 (2007).
[17] M. König, S. Wiedmann, C. Brüne, A. Roth, H. Buhmann, L. W. Molenkamp, X.-L. Qi, and S.-C. Zhang, Science **318**, 766 (2007).
[18] Y. L. Chen, J. G. Analytis, J.-H. Chu, Z. K. Liu, S.-K. Mo, X. L. Qi, H. J. Zhang, D. H. Lu, X. Dai, Z. Fang, S. C. Zhang, I. R. Fisher, Z. Hussain, and Z.-X. Shen, Science **325**, 178 (2009).
[19] A. P. Schnyder, S. Ryu, A. Furusaki, and A. W. W. Ludwig, Phys. Rev. B **78**, 195125 (2008).
[20] W. P. Su, J. R. Schrieffer, and A. J. Heeger, Phys. Rev. Lett. **42**, 1698 (1979).
[21] W. P. Su, J. R. Schrieffer, and A. J. Heeger, Phys. Rev. B **22**, 2099 (1980).
[22] M. Xiao, Z. Q. Zhang, and C. T. Chan, Phys. Rev. X **4**, 021017 (2014).
[23] N. W. Ashcroft and N. D. Mermin, *Solid State Physics* (Holt, Rinehart and Winston, New York, 1976).
[24] D. Vanderbilt, *Berry Phases in Electronic Structure Theory: Electric Polarization, Orbital Magnetization and Topological Insulators* (Cambridge University Press, Cambridge, 2018).
[25] J. Zak, Phys. Rev. Lett. **62**, 2747 (1989).
[26] D. Vanderbilt and R. D. King-Smith, Phys. Rev. B **48**, 4442 (1993).
[27] S. Gangadharaiah, L. Trifunovic, and D. Loss, Phys. Rev. Lett. **108**, 136803 (2012).
[28] J.-H. Park, G. Yang, J. Klinovaja, P. Stano, and D. Loss, Phys. Rev. B **94**, 075416 (2016).
[29] M. Thakurathi, J. Klinovaja, and D. Loss, Phys. Rev. B **98**, 245404 (2018).
[30] T. Ozawa, H. M. Price, A. Amo, N. Goldman, M. Hafezi, L. Lu, M. C. Rechtsman, D. Schuster, J. Simon, O. Zilberberg, and I. Carusotto, Rev. Mod. Phys. **91**, 015006 (2019).
[31] J. K. Asbóth, L. Oroszlány, and A. Pályi, *A Short Course on Topological Insulators* (Springer, 2016).
[32] D. J. Thouless, Phys. Rev. B **27**, 6083 (1983).
[33] A. A. Cottey, Am. J. Phys. **39**, 1235 (1971).
[34] See Supplemental Material at [URL will be inserted by publisher] for detailed information of the transfer-matrix method, comparison of theoretical and experimental transmission data, characterization of localized states, full reflection properties of the semi-infinite systems, and winding direction of complex reflection amplitudes.
[35] R. E. Collin, *Foundations for microwave engineering*, 2nd ed. (McGraw-Hill, New York, 1996).